
Don't be so negative! Score-based Generative Modeling with Oracle-assisted Guidance

Saeid Naderiparizi
Department of Computer Science
University of British Columbia
saeidnp@cs.ubc.ca

Xiaoxuan Liang
Department of Computer Science
University of British Columbia
liang51@cs.ubc.ca

Berend Zwartsenberg
Inverted AI
berend.zwartsenberg@inverted.ai

Frank Wood*
Department of Computer Science
University of British Columbia
fwood@cs.ubc.ca

Abstract

The maximum likelihood principle advocates parameter estimation via optimization of the data likelihood function. Models estimated in this way can exhibit a variety of generalization characteristics dictated by, e.g. architecture, parameterization, and optimization bias. This work addresses model learning in a setting where there further exists side-information in the form of an oracle that can label samples as being outside the support of the true data generating distribution. Specifically we develop a new denoising diffusion probabilistic modeling (DDPM) methodology, Gen-neG, that leverages this additional side-information. Our approach builds on generative adversarial networks (GANs) and discriminator guidance in diffusion models to guide the generation process towards the positive support region indicated by the oracle. We empirically establish the utility of Gen-neG in applications including collision avoidance in self-driving simulators and safety-guarded human motion generation.

1 Introduction

What should we do when we train a generative model that produces samples that we know are “bad” or “not allowed?” Let’s say we have, as is typical, a set of “good” training data samples and additionally an oracle that tells whether a sample is “bad.” We typically maximize the likelihood of “good” samples under our learned generative model. As most models only approximate the true data generating process, often when sampling from a fully trained, highly expressive model, some fraction of generated samples fall in the “bad” region as indicated by the oracle. Assuming the veracity of the oracle, this is a clear indication of model misspecification in the sense of incorrect generalization.

The most natural thing to do with such a model is to deploy it in a rejection sampling loop in which the oracle is used to decide whether to reject a sample or not. Depending on circumstances this may be an acceptable final “generative model,” but it may come at an unacceptable computational cost, particularly in terms of latency. Consider the concrete example of realtime autonomous vehicle model predictive control and path planning [17]. Selecting a control action conditioned on a joint sample of forward in time trajectories that do not produce collisions or other infractions is a supremely important task that requires low latency and extremely high success rates. If a generative model fit on trajectories with no observed collisions or infractions produces infracting joint trajectories with probability ϵ

*Frank Wood is also affiliated with the Montréal Institute for Learning Algorithms (Mila) and Inverted AI.

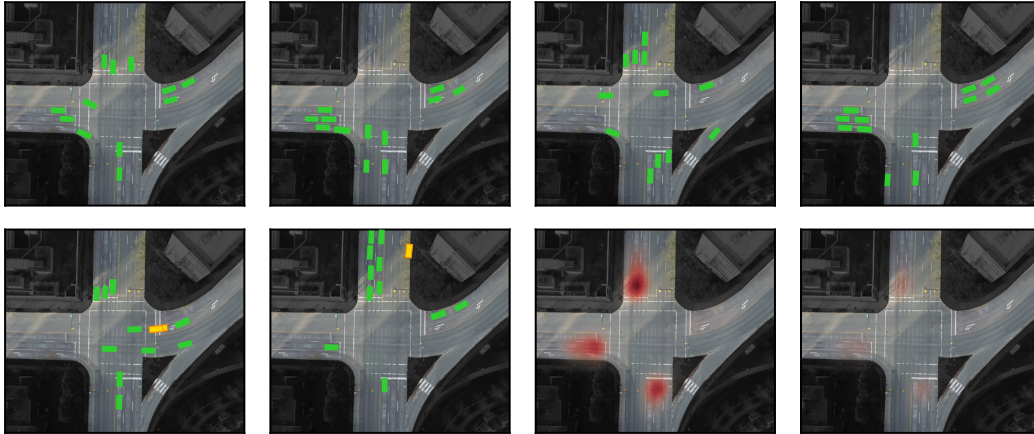


Figure 1: Gen-neG applied to a diffusion model of non-infracting static vehicle placements (i.e. diffusing in the space of a set of oriented rectangles) for the efficient initialization of autonomous vehicle planning simulators (see [49] for a similar model and full problem description). The top row shows samples (green “cars”) that are not colliding (non-overlapping) and not off-road (stay within the unshaded area of road surfaces) from a baseline diffusion model improved by Gen-neG. The second row shows the kind of infractions our oracle identifies as not being in the support of the true distribution; left-most: a collision (yellow overlapping “cars”), second from left: (yellow off-road “car”). The second to right and rightmost figures graphically illustrate the reduction in infractions per unit area before (left) and after Gen-neG is applied to the baseline model (both plots are normalized to the same maximum value). Quantitative results corresponding to this plot appear in Table 1.

(state of the art models [22, 10, 13, 7, 27, 33] can have high joint infraction rates), then in order to find at least one non-infracting sample with $1 - \delta$ probability without looping the rejection sampler requires $\frac{\log \delta}{\log \epsilon}$ batched parallel samples. Depending on the specific concrete value of $1 - \delta$ required (e.g. 1 chance in a billion of having latency arising from rejection sampling looping imposed) and the baseline trajectory model rejection rate (e.g. 30-50% is not atypical) this could require running many parallel samplers (in this concrete example around 30), a number that, depending on model size and available realtime edge computational capacity, is likely to be prohibitively large. Other concrete examples of this nature arise in many control as inference problems [23]. Minimizing ϵ directly, or restricting the generative model to only place mass on the positive support region indicated by the oracle, is the most natural thing to try to combat this problem. Working towards this goal includes a body of work on amortized rejection sampling [26, 43] and the body of related work on generative adversarial networks (GAN)s [11]. Of course in the GAN setting the discriminator (which can be used in a rejection sampling loop for improved performance [3, 6]) is learned rather than being fixed as in the case we consider.

Modern highly expressive deep generative models are sufficiently parameterized and easy to optimize so that they can effectively be trained to result in the de facto non-parametric optimal maximum likelihood solution of placing a mixture of Dirac measures directly on the training data. Transformer-based [41] denoising diffusion process models [35, 15] are one-such model class. Such models must be either trained on tremendously large amounts of data [32] or otherwise “de-tuned” (smaller architecture, fewer integration steps, etc.) to ensure that they generalize rather than memorize [48, 2]. In this paper we are agnostic to this point and assume that we are operating in a realistic modeling regime where the model generalizes. Our work can be seen as a way to control the specific kind of generalization that the model exhibits.

We focus specifically on diffusion models, which present several possible ways to solve this problem. While there are a multitude of options that could be considered for this problem, we only report one in this work. We mention but don’t formally report these explorations in Appendix C.1 to combat the positive-results-only bias in our literature that leads to wasted duplicated research time and effort.

What we discovered, and report in this work, is a *simple rule for classifier guidance* that has been seemingly, to the best of our knowledge, surprisingly overlooked. Drawing inspiration from results in

the very recent work on discriminator guidance in diffusion processes [19] (the marriage of diffusion processes with GAN discriminator losses), we establish a new methodology for classifier guidance that learns and uses a sequence of differentiable classifiers fit to synthetic samples labelled by the oracle drawn from a sequence of classifier guided diffusion models. The resulting sequence of multiply classifier guided diffusion models (or the end of a sequence of distilled models; details to follow) monotonically decreases the rejection rate while empirically maintaining a competitive probability mass assigned to validation samples. The key insight and technical contribution boils down to a carefully choosing the ratio of “good” and “bad” synthetic samples to use when training each of the sequence of guidance classifiers.

We demonstrate our methodology, which we call **Generative modeling with neGative examples** (Gen-neG) on several problems, including modeling motion capture sequence data in a way that eliminates ground plane violations and static traffic scene vehicle arrangements that avoid collisions and off-road placements. We empirically demonstrate that Gen-neG can drive the ratio of samples that violate the constraint set monotonically towards zero, while maintaining or even increasing (as one would expect from renormalizing a probability distribution from shifting mass away from the no-support region specified by the oracle) the probability assigned to held out validation samples.

2 Background

2.1 Score-based Diffusion Models

Score-based diffusion models [35, 37, 15, 38], also referred to as diffusion models (DMs) are a class of generative models that are defined through a stochastic process which gradually adds noise to samples from a data distribution $q_0(\mathbf{x}_0)$, such that when simulated forward from $t = 0$ the marginal distribution at time T is $q_T(\mathbf{x}_T) \approx \pi(\mathbf{x}_T)$ for some known $\pi(\mathbf{x}_T)$ typically equal to $\mathcal{N}(\mathbf{0}, \mathbf{I})$. This is known as the “forward process” and is formulated as an SDE

$$d\mathbf{x}_t = f(\mathbf{x}_t, t)dt + g(t)d\mathbf{w}, \quad \mathbf{x}_0 \sim q_0(\mathbf{x}_0) \quad (1)$$

where f and g are predefined drift and diffusion coefficients of \mathbf{x}_t and \mathbf{w} is the standard Wiener process. DMs generate data by learning the inverse of this process, which is known as the “reverse process” and defined as

$$d\mathbf{x}_t = [f(\mathbf{x}_t, t) - g(t)^2 s_\theta(\mathbf{x}_t; t)]d\bar{t} + g(t)d\bar{\mathbf{w}}, \quad \mathbf{x}_T \sim \pi(\mathbf{x}_T), \quad (2)$$

where \bar{t} and $\bar{\mathbf{w}}$ are the infinitesimal reverse time and reverse Wiener process, respectively. If s_θ approximates the score function of the marginals of the forward process, the terminal distribution of the reverse process coincides with $q_0(\mathbf{x}_0)$ [1]. Formally, when

$$s_\theta(\mathbf{x}_t; t) = \nabla_{\mathbf{x}_t} \log q_t(\mathbf{x}_t) \quad (3)$$

we have

$$p_\theta(\mathbf{x}_0; 0) = q_0(\mathbf{x}_0), \quad (4)$$

where $p_\theta(\mathbf{x}_t; t)$ is the marginal distribution of the approximate reverse process.

In order to approximate the score function $\nabla_{\mathbf{x}_t} \log q_t(\mathbf{x}_t)$, DMs minimize the following score matching objective function [16, 42, 37]:

$$\mathcal{L}_\theta^{\text{DM}} = \mathbb{E}_{t, \mathbf{x}_0, \mathbf{x}_t} \left[\gamma_t \|s_\theta(\mathbf{x}_t; t) - \nabla_{\mathbf{x}_t} \log q(\mathbf{x}_t | \mathbf{x}_0)\|^2 \right], \quad (5)$$

where $\mathbf{x}_0 \sim q(\mathbf{x}_0)$, $\mathbf{x}_t \sim q(\mathbf{x}_t | \mathbf{x}_0)$, t is sampled from a distribution over $[0, T]$, and γ_t is a positive weighting term. Importantly, the Wiener process in Eq. (1) allows direct sampling from the marginals of the forward distributions [38], i.e. $q(\mathbf{x}_t | \mathbf{x}_0) = \mathcal{N}(\alpha_t \mathbf{x}_0, \sigma_t)$, with α_t and σ_t determined by the drift and diffusion coefficients in Eq. (1). This formulation moreover allows the evaluation of the score function ($\nabla_{\mathbf{x}_t} \log q(\mathbf{x}_t | \mathbf{x}_0)$) in closed form.

Many of the DMs reported in the literature operate on discrete time steps [15, 36, 28], and can be considered as particular discretizations of the presented framework. Various parameterizations of the score function have been also explored in the literature.

In the remainder of this paper we use q to denote the forward process, s_θ for the score function of the reverse process and p_θ is the distribution generated by running Eq. (2) backward in time. This applies to the marginals, conditionals, and posteriors as well. Furthermore, to avoid unnecessary notation clutter throughout the rest of the paper, we omit the explicit mention of θ and ϕ and t when their meaning is evident from the context.

2.2 Classifier Guidance

A distinctive and remarkable property of DMs is the ability to train an unconditional version and sample from its class-conditional distributions at inference time without requiring re-training or fine-tuning [9, 38]. However, it requires a time-dependent classifier $q(y|\mathbf{x}_t) = \int q(y|\mathbf{x}_0)q(\mathbf{x}_0|\mathbf{x}_t)$. Here, $q(y|\mathbf{x}_0)$ is a traditional classifier, that predicts the class probabilities for each y given a datum \mathbf{x}_0 from the dataset. While $q(y|\mathbf{x}_t)$ classifies a noisy datum \mathbf{x}_t sampled from $q_t(\mathbf{x}_t) = \int q(\mathbf{x}_t|\mathbf{x}_0)q(\mathbf{x}_0) d\mathbf{x}_0$.

Classifier guidance follows from the identity $\nabla_{\mathbf{x}_t} \log q(\mathbf{x}_t|y) = \nabla_{\mathbf{x}_t} \log q(\mathbf{x}_t) + \nabla_{\mathbf{x}_t} \log q(y|\mathbf{x}_t)$. If $s_\theta(\mathbf{x}_t; t)$ is the score function of the DM, then the score function of the class-conditional DM is

$$s_\theta(\mathbf{x}_t|y; t) = s_\theta(\mathbf{x}_t; t) + \nabla_{\mathbf{x}_t} \log q(y|\mathbf{x}_t). \quad (6)$$

Binary classification A special case of the above classifier guidance that we use in this paper is when there are only two classes. We provide here a brief overview of such a binary classification task and the notation associated with it. Let $q(\mathbf{x}|y=1)$ and $q(\mathbf{x}|y=0)$ be the distribution of positive and negative examples. Let α and $1-\alpha$ be the prior probabilities $q(y)$ of positive and negative examples. We then have $q(\mathbf{x}) = q(y=1)q(\mathbf{x}|y=1) + q(y=0)q(\mathbf{x}|y=0) = \alpha q(\mathbf{x}|y=1) + (1-\alpha)q(\mathbf{x}|y=0)$. A binary classifier $C_\phi : \mathcal{X}, [0, T] \rightarrow [0, 1]$, can then be trained to approximate $q(y=1|\mathbf{x}_t)$ by minimizing the expected cross-entropy loss

$$\mathcal{L}_\phi^{\text{CE}} = -\mathbb{E}_t \left[\mathbb{E}_{q(\mathbf{x}_t)} [q(y=1|\mathbf{x}_t) \log C_\phi(\mathbf{x}_t; t) + q(y=0|\mathbf{x}_t) \log(1 - C_\phi(\mathbf{x}_t; t))] \right]. \quad (7)$$

Minimizing the cross-entropy loss between the classifier output and the true label is equivalent to minimizing the KL divergence between the classifier output and the Bayes optimal classifier (see Appendix A.3). The minimizer of this loss is then

$$C_{\phi^*}(\mathbf{x}_t; t) = \frac{\alpha q(\mathbf{x}_t|y=1)}{\alpha q(\mathbf{x}_t|y=1) + (1-\alpha)q(\mathbf{x}_t|y=0)}. \quad (8)$$

3 Methodology

In this section, we describe **Generative modelling with neGative examples (Gen-neG)**. Gen-neG makes use of an oracle that can distinguish samples that are outside of the support for the problem. In a nutshell, Gen-neG consists of first training a DM on given training data as usual, (we refer to the resulting DM as the “baseline DM” throughout). Then we draw samples from this baseline DM, label them using the oracle, then train a classifier (for guidance) using those samples, critically, as we will demonstrate, ensuring that the correct ratio of positive and negative examples are used in training. We then combine this classifier and the baseline model in the typical classifier guidance way. Gen-neG establishes this classifier guided DM as a new baseline DM (either fixing and ultimately “stacking” classifiers or optionally distilling the classifier guided DM into a DM with a single score function estimator) and then repeats this process of generating samples from this new baseline, labelling them with the oracle, training a classifier with the carefully chosen label ratio, employing classifier guidance, stacking or distilling, then repeating. Throughout we will refer to the resulting DM as stacked or distilled depending on whether or not distillation into a unified score function is employed.

3.1 Problem formulation and notation

Let $\mathcal{D} = \{\mathbf{x}^i\}_{i=1}^N \sim q(\mathbf{x})$ be a dataset of i.i.d. samples from an unknown data distribution q . Furthermore, let $\mathcal{O} : \mathcal{X} \rightarrow \{0, 1\}$ be an oracle function that assigns each point in the data space \mathcal{X} a binary label. In other words, this oracle partitions the data space into two disjoint sets $\mathcal{X} = \Omega \cup \Omega^{\mathcal{O}}$ such that $\mathcal{O}(\mathbf{x}) = \mathbf{1}_\Omega(\mathbf{x})$. Our objective is to learn a score-based diffusion model that (1) maximizes the likelihood of \mathcal{D} and (2) avoids allocating probability to $\Omega^{\mathcal{O}}$.

In the first stage of Gen-neG we train a DM, $p_\theta(\mathbf{x})$, following standard DM training procedures (e.g. Section 2.1) without utilizing the oracle. In the second stage, we leverage the oracle to train a binary classifier that guides the generation process of DM to avoid $\Omega^{\mathcal{O}}$. We explain this second stage in the rest of this section.

Algorithm 1 Gen-neG

Input: dataset \mathcal{D} , oracle \mathcal{O} , balanced synthetic dataset size N
 $i \leftarrow 0$
 $\theta_i \leftarrow \arg \min_{\theta} \mathcal{L}_{\theta}^{\text{DM}}$ ▷ train baseline DM, Eq. (5)
 $s_i \leftarrow s_{\theta_i}(\mathbf{x}_t; t)$
while not done **do**
 $\mathcal{D}_i^+, \mathcal{D}_i^- \leftarrow$ generate samples from DM with score function s_i and label with \mathcal{O}
 while $\min(|\mathcal{D}_i^+|, |\mathcal{D}_i^-|) < N$ **do**
 $\mathcal{D}^+, \mathcal{D}^- \leftarrow$ generate more samples from DM with score function s_i and label with \mathcal{O}
 $\mathcal{D}_i^+ \leftarrow \mathcal{D}_i^+ \cup \mathcal{D}^+, \mathcal{D}_i^- \leftarrow \mathcal{D}_i^- \cup \mathcal{D}^-$
 end while
 $\alpha_i \leftarrow |\mathcal{D}_i^+| / (|\mathcal{D}_i^+| + |\mathcal{D}_i^-|)$ ▷ Estimate class prior probabilities for Bayes optimal classifier
 $\mathcal{D}_i^+ \leftarrow \text{select}(N, \mathcal{D}_i^+), \mathcal{D}_i^- \leftarrow \text{select}(N, \mathcal{D}_i^-)$ ▷ balance dataset for IS classifier training
 $\phi_i \leftarrow \arg \min_{\phi} \hat{\mathcal{L}}_{\phi}^{\text{cls}}(\alpha_i, \mathcal{D}_i^+, \mathcal{D}_i^-)$ ▷ train guidance classifier, Eq. (13)
 $i \leftarrow i + 1$
 if distill **then**
 $\psi \leftarrow \arg \min_{\psi} \mathcal{L}_{\psi}^{\text{dtl}}$ ▷ distill into single DM, Eq. (14)
 $s_i \leftarrow s_{\psi}(\mathbf{x}_t; t)$
 else ▷ “stack” guidance classifiers
 $s_i \leftarrow s_{i-1} + \nabla_{\mathbf{x}_t} \log C_{\phi_i}(\mathbf{x}_t; t)$ ▷ See Eq. (9)
 end if
end while
return DM score function s_i

3.2 Bayes Optimal Classifier Guidance for Diffusion models

The core component of Gen-neG is a classifier that discriminates between positive and negative samples respectively in Ω and $\Omega^{\mathcal{G}}$, which is used to guide the baseline DM. There are two main insights required for Gen-neG that our work provides, the first of which is how to obtain the correct distribution of training data for such a classifier and the second is how to train a classifier which does not shift the sampling distribution.

Oracle-assisted classifier guidance Classifier guidance in score-based models is typically used to generate samples from a specific pre-defined class on the training dataset. For instance, a classifier trained on an image classification dataset can be utilized to guide an unconditional diffusion model that has been trained on the same dataset. Unlike traditional approaches that rely on explicit, predefined, labelled datasets, our framework operates based on the oracle function $\mathcal{O}(\mathbf{x})$, which determines the validity of samples.

Gen-neG instead builds a binary classification task using the fully-synthetic data generated by the baseline DM i.e. the data is distributed as $p_{\theta}(\mathbf{x})$ and the labels are $y = \mathcal{O}(\mathbf{x})$. A time-dependent binary classifier C_{ϕ} is then trained on this dataset. Finally the classifier is incorporated into the baseline DM by

$$s_{\theta, \phi}(\mathbf{x}_t; t) = s_{\theta}(\mathbf{x}_t; t) + \nabla_{\mathbf{x}_t} \log C_{\phi}(\mathbf{x}_t; t). \quad (9)$$

Equivalently, we denote the marginal distributions generated by the oracle-assisted DM as $\tilde{p}_{\theta, \phi}(\mathbf{x}_t; t)$. In the rest of this section we show why the classifier guidance in $\tilde{s}_{\theta, \phi}$ helps to enhance the model and reduce the amount of mass on $\Omega^{\mathcal{G}}$, i.e. $\int_{\mathbf{x} \in \Omega^{\mathcal{G}}} p_{\theta, \phi^*}(\mathbf{x})$.

Theorem 1. *Let $p_{\theta}(\mathbf{x})$ be the distribution learned by a baseline DM with marginal distributions denoted by $p_{\theta}(\mathbf{x}_t; t)$ and let $p_{\theta}(y = 1 | \mathbf{x}_0) = \mathcal{O}(\mathbf{x}_0)$. Further, let $C_{\phi^*} : \mathcal{X}, [0, T] \rightarrow [0, 1]$ be the Bayes-optimal time-dependent binary classifier arising from perfectly optimizing the following cross-entropy objective*

$$\mathcal{L}_{\phi}^{\text{CE}} = -\mathbb{E}_t [\mathbb{E}_{p_{\theta}(\mathbf{x}_0, \mathbf{x}_t)} [\mathcal{O}(\mathbf{x}_0) \log C_{\phi}(\mathbf{x}_t; t) + (1 - \mathcal{O}(\mathbf{x}_0)) \log(1 - C_{\phi}(\mathbf{x}_t; t))]] \quad (10)$$

then

$$\nabla_{\mathbf{x}_t} \log p_{\theta}(\mathbf{x}_t; t) + \nabla_{\mathbf{x}_t} \log C_{\phi^*}(\mathbf{x}_t; t) = \nabla_{\mathbf{x}_t} \log p_{\theta}(\mathbf{x}_t | y = 1; t). \quad (11)$$

In other words, by using a Bayes-optimal binary classifier for guidance, we target exactly the score function of positive (oracle-approved) examples.

Corollary 1.1. For an optimal classifier C_{ϕ^*} ,

1. $p_{\theta, \phi^*}(\mathbf{x}) = p_{\theta}(\mathbf{x}|y = 1)$,
2. There is no mass on Ω^c , i.e. $\int_{\mathbf{x} \in \Omega^c} p_{\theta, \phi^*}(\mathbf{x}) = 0$,
3. For any dataset $\mathcal{D} \subseteq \Omega$, $p_{\theta, \phi^*}(\mathcal{D}) \geq p_{\theta}(\mathcal{D})$.

Corollary 1.1 suggests the guidance our Gen-neG methodology can improve the baseline DM in terms of both infraction rate and test dataset likelihood.

See the proofs for the Theorem 1 and Corollary 1.1 in Appendices A.1 and A.2.

Training the classifier Training the classifier in our approach presents a noteworthy challenge due to the major label imbalance within the synthetic dataset \mathcal{D} generated by the model. This imbalance emerges because the baseline is already close to the target distribution, resulting in a scarcity of negative examples. However, these negative examples play a crucial role in guiding the model at the boundary between positive and negative examples, where the model requires the most guidance.

Gen-neG addresses this challenge by sampling a balanced dataset \mathcal{D} from the model, ensuring the same number of positive and negative examples. However, Gen-neG crucially employs importance sampling in the classifier’s training objective to rectify the bias introduced by having to balance the dataset to achieve high classifier accuracy in training. Theorem 1 suggests that a classifier trained on dataset whose marginal distribution over labels differs from the true marginal distribution over labels will target the wrong cross-entropy and arrive at a classifier guided DM that does not necessarily target the distribution of interest. We show evidence of this happening in Fig. 2.

Finally, in order to avoid the computational cost of sampling from the baseline DM to compute the classifier objective in Eq. (10), we approximate the $p(\mathbf{x}_0, \mathbf{x}_t) = p(\mathbf{x}_0)p(\mathbf{x}_t|\mathbf{x}_0) \approx p(\mathbf{x}_0)q(\mathbf{x}_t|\mathbf{x}_0)$. This is similar to the approximation in Kim et al. [19]. In particular, the classifier’s objective in Gen-neG is

$$\begin{aligned} \mathcal{L}_{\phi}^{\text{cls}}(\alpha) := & \alpha \mathbb{E}_{p_{\theta}(\mathbf{x}_0|y=1)} \left[\mathbb{E}_{q(\mathbf{x}_t|\mathbf{x}_0)} [-\log C_{\phi}(\mathbf{x}_t; t)] \right] \\ & + (1 - \alpha) \mathbb{E}_{p_{\theta}(\mathbf{x}_0|y=0)} \left[\mathbb{E}_{q(\mathbf{x}_t|\mathbf{x}_0)} [-\log(1 - C_{\phi}(\mathbf{x}_t; t))] \right]. \end{aligned} \quad (12)$$

Given the balanced dataset $\mathcal{D} = \mathcal{D}^+ \cup \mathcal{D}^-$ where $\mathcal{D}^+ \sim p(\mathbf{x}_0|y = 1)$, $\mathcal{D}^- \sim p(\mathbf{x}_0|y = 0)$, and $N = |\mathcal{D}^+| = |\mathcal{D}^-|$,

$$\begin{aligned} \hat{\mathcal{L}}_{\phi}^{\text{cls}}(\alpha, \mathcal{D}^+, \mathcal{D}^-) := & \frac{1}{N} \sum_{\mathbf{x}_0 \in \mathcal{D}^+} \alpha \mathbb{E}_{q(\mathbf{x}_t|\mathbf{x}_0)} [-\log C_{\phi}(\mathbf{x}_t; t)] \\ & + \frac{1}{N} \sum_{\mathbf{x}_0 \in \mathcal{D}^-} (1 - \alpha) \mathbb{E}_{q(\mathbf{x}_t|\mathbf{x}_0)} [-\log(1 - C_{\phi}(\mathbf{x}_t; t))], \end{aligned} \quad (13)$$

is an importance sampling estimator of the objective function in Eq. (12); proof in Appendix A.5.

Iterative Training by Stacking Classifiers If the classifier is perfect, we know that the DM with score function $s_{\theta, \phi}$ will have improved likelihood and zero infraction (see Corollary 1.1). However, in practice the trained classifier is only an estimate and infractions may not be entirely eliminated.

To alleviate this problem, we note that once the classifier is trained the guided score function $s_{\theta, \phi}(\mathbf{x})$ itself defines a new diffusion model. Consequently, we can employ a similar procedure to train a new classifier on $s_{\theta, \phi}$, aiming to further lower its infraction rate. This iterative approach involves training successive classifiers and incorporating them into the model, progressively enhancing its performance and reducing the infraction rate.

Distillation Adding a stack of classifiers to the model linearly increases its computational cost, since each new classifier requires a forward and backward pass each time the score function is evaluated. To avoid this, we propose to distill the classifiers into the baseline model.

Let $s_{\theta, \Phi}$ be a “teacher model” consisting of a baseline model s_{θ} and a stack of classifiers $\{C_{\phi}\}_{\phi \in \Phi}$. We distill $s_{\theta, \Phi}$ into a new “student model” s_{ψ}^{dl} , possibly with the same architecture as the baseline

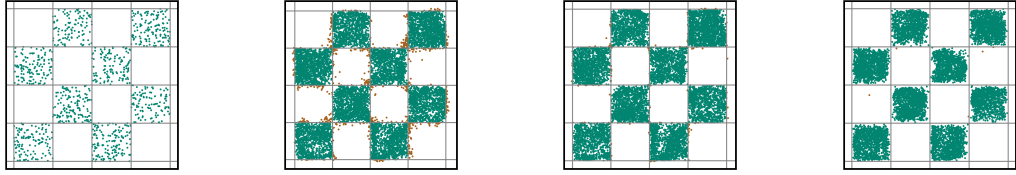


Figure 2: Samples from the toy experiment. Samples with infraction (i.e. $\mathcal{O}(\mathbf{x}) = 0$) are shown in brown. From left to right: The true dataset; baseline DM; first iteration of Gen-neG using a label distribution of equal proportions in guidance classifier training. Using the wrong distribution to train classifier guidance results in suboptimal density estimation. Here we see that samples are suboptimally pushed inwards from the boundaries. We also have observed that validation ELBOs in these kinds of cases are significantly worse.

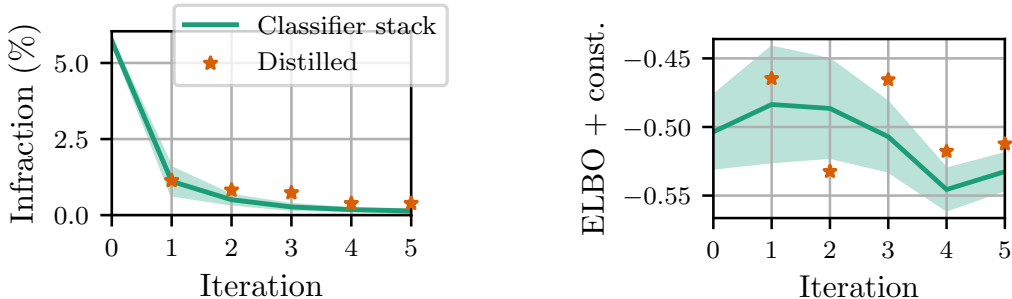


Figure 3: Infraction and ELBO estimations from different iterations of Gen-neG. The infraction rate keeps decreasing, and ELBO remains comparable for the first few iterations. Orange stars show the performance of the model after distillation. We only observe a minor loss of performance in the distilled models. In comparison, without applying importance sampling (the rightmost panel of Fig. 2) reaches an infraction of 0.03% but ELBO of -1.42 .

model, by minimizing the following distillation loss

$$\mathcal{L}_{\psi}^{\text{dtl}} = \mathbb{E}_{\mathbf{x}_0 \sim q(\mathbf{x}_0), t} \left[\gamma_t \left\| s_{\theta, \Phi}(\mathbf{x}_t; t) - s_{\psi}^{\text{dtl}}(\mathbf{x}_t; t) \right\|^2 \right], \quad (14)$$

where γ_t is the weight term, similar to the training objective of diffusion models. Here, \mathcal{L}^{dtl} makes the outputs of the student model match that of the teacher. Algorithm 1 summarises Gen-neG.

4 Experiments

We demonstrate Gen-neG on three datasets: a 2D checkerboard, collision avoidance in traffic scenario generation for and safety-guarded human motion generation. In each experiment we report a likelihood-based metric on a held out dataset to measure distributional shifts and a kind of infraction metric to measure faithfulness to the oracle.

4.1 Toy Experiment

We first demonstrate Gen-neG on a simple dataset of 2D points uniformly distributed on a checkerboard grid as shown in Fig. 2. We apply EDM [18], a continuous-time DM, to this problem. A baseline DM trained for long enough on this dataset can easily achieve negligible infraction rate. However, because our dataset (see the first panel of Fig. 2) only contains 1000 points the model is prone to over-fitting (see Appendix C.4 for overfitting results). We therefore stop training of the baseline DM before it starts overfitting measured by the evidence lower bound (ELBO) on a held-out validation set. The second panel of Fig. 2 shows samples drawn from the baseline DM and the third panel shows the improved results after one iteration of Gen-neG. We further report in Fig. 3 the rate

Table 1: Results for traffic scene generation, in terms of collision, offroad, and overall infractions as well as ELBO. Two varieties (“by-scene” and “by-agent”) for the classifier are presented, as well as results with (Gen-neG) and without importance sampling. The final two rows provide the results of distilling the models labelled with † and *.

Method	Collision (%) ↓	Offroad (%) ↓	Infraction (%) ↓	r-ELBO ($\times 10^2$) ↑
baseline DM	28.3 ± 0.70	1.3 ± 0.14	29.3 ± 0.64	−27.5 ± 0.01
by-scene w/o IS	20.5 ± 1.21	0.9 ± 0.17	21.9 ± 1.14	−27.7 ± 0.01
by-scene	23.3 ± 0.7	1.0 ± 0.28	24.1 ± 0.67	−27.6 ± 0.01
by-agent w/o IS	14.6 ± 0.49	0.8 ± 0.13	15.2 ± 0.50	−28.0 ± 0.01
by-agent†	16.4 ± 0.5	0.9 ± 0.12	17.2 ± 0.44	−27.7 ± 0.01
by-agent stacked*	11.6 ± 0.65	0.6 ± 0.10	12.2 ± 0.60	−28.0 ± 0.01
Distillation of (†)	12.2 ± 0.42	0.8 ± 0.06	12.9 ± 0.36	−26.8 ± 0.01
Distillation of (*)	5.1 ± 0.24	0.5 ± 0.09	5.6 ± 0.20	−27.0 ± 0.01

of oracle violation $\int_{\mathbf{x} \in \Omega_c} p_{\theta, \phi^*}$, which we will refer to as the infraction rate, and an ELBO estimate by the trained model after each iteration for up to 5 iterations. It demonstrates each iteration of Gen-neG, improves the infraction rate with a comparable ELBO, at least for the first few iterations. Fig. 3 also shows that distillation does not lead to a significant drop in performance.

We also report results for an experiment of one iteration of classifier guidance without the application of proper importance sampling (IS) weights. In this case, the classifier is trained on a synthetic dataset with a uniform class distribution. The last panel of Fig. 2 visualizes samples from this model. While method produces an excellent infraction rate of about 0.03%, the classifier severely modifies the shape of the distribution, an undesirable side effect. In particular, we can see the areas close to the boundary have strongly reduced density. In quantitative terms, we find that the ELBO of this imbalanced classifier approach is −1.42, a significantly worse result.

4.2 Infractions in Traffic Scene Generation

We consider the task of traffic scene generation, where vehicles of variable size, are placed on a two dimensional map with according orientations. Traditionally implemented by as rule based systems [46, 25], this task has recently been approached using generative modelling techniques [39, 49]. The approach taken in both these bodies of prior art is to reject any infracting samples, which in this case means a vehicle is off the driving area (“offroad”), or overlaps with another (“collision”). While rejecting such samples is generally effective, it is computationally wasteful, especially when the rate of infractions is high. We therefore apply Gen-neG to this task, in order to improve performance. The specific task we consider is to generate N vehicles in a given scene, conditioned on a rendered representation of the drivable area. For each vehicle, the position, length, width, orientation and velocity are predicted for a total of 7 dimensions per vehicle. Vehicles are sampled *jointly*, meaning that the overall distribution $p_{\theta}(\mathbf{x}) \mathbf{x} \in \mathbb{R}^{N \times 7}$. We train the baseline employing the formalism in DDPM [15] with a transformer-based denoising network [41] on a private dataset. Our architecture consists of self-attention layers and map-conditional cross-attention layers in an alternating order. We use relative positional encodings (RPEs) [34, 45], which makes use of the vehicles relative positions. Relevant samples (including infracting, and non-infracting ones) and road geometry can be seen in Fig. 1. For our experiments, the oracle function either assigns each scene a collective label, or for each vehicle an individual label. This label is based on the occurrence of collisions or offroad infractions. We then use these results to construct “by-scene” and “by-agent” classifiers.

Table 1 presents the results of our experiments. We provide results for both the “by-agent” and “by-scene” experiments, both showing significant improvement over the baseline result. We moreover show ablations for both settings, where we drop the importance sampling (“w/o IS”), which results in improved infraction rates, but a decreased ELBO. We also provide results for a multi-round approach in the “by-agent” setting, which shows even better results. Finally, we demonstrate that our approach of distilling the resulting models back into a single one works well here too, albeit at a slight drop in performance on ELBO. Overall we find that Gen-neG works as expected, and provides a competitive infraction rate boost over our baseline model, without sacrificing likelihood performance.

Table 2: Results of the Motion Diffusion experiment. “Inf. per step” is the average rate of generated motion frames with infraction while “infraction” is the average rate of generated motions that at least including one infracting frame. r-ELBO is a reweighted ELBO with the same weighting as in diffusion loss.

Method	Infraction (%) ↓	Inf. per step (%) ↓	r-ELBO ($\times 10^2$) ↑	FID ↓
MDM	18.92 ± 0.58	4.55 ± 0.03	-6.03 ± 0.04	0.783
MDM + classifier	15.35 ± 0.53	3.15 ± 0.02	-7.25 ± 0.11	0.822
MDM + classifier w/o IS	13.38 ± 0.50	2.40 ± 0.02	-9.19 ± 0.30	1.040

4.3 Motion Diffusion

Our final experiment is a text-conditional motion generation task on the HumanML3D dataset [12]. The dataset contains 14,616 human motions annotated by 44,970 textual descriptions. It includes motions between 2 and 10 seconds in length and their total length amounts to 28.59 hours. For our baseline DM, we use the pre-trained checkpoints provided by Human Motion Diffusion (MDM) [40]. MDM employs DDPM to learn a transformer-based architecture [41] with a pre-trained CLIP embedding module [30] to facilitate conditioning on the descriptions. It has been shown that, despite its high quality generated motion, under more detailed inspection, MDM and other DMs often lack physical plausibility [47]. For example, ground penetration often exists in the generated examples. Such imperfections can cause issues if the model were to be used in downstream applications. To address this issue, we implement an oracle that labels motions with ground penetration at any point in their duration as negative. We then train our classifier with an architecture that matches that of the original diffusion model with the CLIP encoder removed, because the classifier is not conditioned on the text. We evaluate performance in terms of infraction rate, and the reweighted ELBO, the reweighting referring to a uniform schedule of γ_t in Eq. (5).

Table 2 summarizes our results of one iteration of Gen-neG on this dataset. Gen-neG improves both the per-step and overall infraction rate with a small drop in the reweighted ELBO and FID. While guiding using a classifier trained without IS weighting produces lower infraction rates, the reweighted ELBO and FID in that case drops even further. Hence, Gen-neG provides a significant improvement of the infraction rates, with a lower cost in terms of model likelihood or sample quality.

5 Related Work

Liu et al. [24] employs diffusion bridges to define a family of diffusion models that are guaranteed to be bound to a constrained set Ω by construction. Their approach, however, is limited to constraints that admit tractable expectations, rendering it impractical for any but the simplest constraints such as product of intervals in \mathbb{R}^d . The second one is Kong and Chaudhuri [21] which refers to the problem as “data redaction.” They consider multiple setting, one of which, validity-based approach is mostly related to our oracle-assisted guidance, but in the GAN literature. They implicitly perform data redaction by incorporating them into the discriminator and fine-tune the generator. Last, Kim et al. [19] incorporates a binary classifier in the form of GAN discriminators to refine the the learned distribution of DMs, further improving its sample quality. While they utilize a set of tools similar to ours, the problems we tackle different problems.

6 Conclusion

We have proposed a framework to incorporate constraints into diffusion models. These constraints are defined through an oracle function that categorizes samples as either *good* or *bad*. Importantly, such a flexibility allows for simple integration with human feedback. We have demonstrated our model on different modalities demonstrating how it can benefit safety constraints.

Possible future directions for this work are (1) incorporating the true training dataset into the later iterations of the method, as the training dataset only affects the baseline DM. The next stages solely use synthetic data. Although we show theoretically that our guidance only improves the model, this lack of revisiting the true dataset in presence of practical errors and approximations poses challenges for large-scale adoption of our method. Our preliminary experiments of visiting the true dataset at the

distillation time have not been successful yet. (2) Avoiding stacking of classifiers, instead directly learning an artifact that can replace the previous classifier in our method, similar to [8], is vital to the computational complexity of the method as the current computational cost scales linearly with the number of classifiers. (3) Bridging the gap the diffusion bridge-based approaches and our work which is practically applicable to a larger set of applications is another avenue for future developments.

Acknowledgements

We acknowledge the support of the Natural Sciences and Engineering Research Council of Canada (NSERC), the Canada CIFAR AI Chairs Program, and the Intel Parallel Computing Centers program, and the Mitacs Accelerate program in partnership with Inverted AI. Additional support was provided by UBC’s Composites Research Network (CRN), and Data Science Institute (DSI). This research was enabled in part by technical support and computational resources provided by WestGrid (www.westgrid.ca), Compute Canada (www.computeCanada.ca), and Advanced Research Computing at the University of British Columbia (arc.ubc.ca). We thank Setareh Cohan for helping us with the motion diffusion experiments.

References

- [1] Brian D.O. Anderson. Reverse-time diffusion equation models. *Stochastic Processes and their Applications*, 12(3):313–326, 1982. ISSN 0304-4149. doi: [https://doi.org/10.1016/0304-4149\(82\)90051-5](https://doi.org/10.1016/0304-4149(82)90051-5). URL <https://www.sciencedirect.com/science/article/pii/0304414982900515>.
- [2] Devansh Arpit, Stanisław Jastrzębski, Nicolas Ballas, David Krueger, Emmanuel Bengio, Maxinder S Kanwal, Tegan Maharaj, Asja Fischer, Aaron Courville, Yoshua Bengio, et al. A closer look at memorization in deep networks. In *Proceedings of the 34th International Conference on Machine Learning-Volume 70*, pages 233–242, 2017.
- [3] Samaneh Azadi, Catherine Olsson, Trevor Darrell, Ian Goodfellow, and Augustus Odena. Discriminator rejection sampling. In *International Conference on Learning Representations*, 2018.
- [4] Irwan Bello, Barret Zoph, Ashish Vaswani, Jonathon Shlens, and Quoc V Le. Attention augmented convolutional networks. In *Proceedings of the IEEE/CVF international conference on computer vision*, pages 3286–3295, 2019.
- [5] Nicolas Carion, Francisco Massa, Gabriel Synnaeve, Nicolas Usunier, Alexander Kirillov, and Sergey Zagoruyko. End-to-end object detection with transformers. In *Computer Vision—ECCV 2020: 16th European Conference, Glasgow, UK, August 23–28, 2020, Proceedings, Part I 16*, pages 213–229. Springer, 2020.
- [6] Tong Che, Ruixiang Zhang, Jascha Sohl-Dickstein, Hugo Larochelle, Liam Paull, Yuan Cao, and Yoshua Bengio. Your gan is secretly an energy-based model and you should use discriminator driven latent sampling. *Advances in Neural Information Processing Systems*, 33:12275–12287, 2020.
- [7] Henggang Cui, Vladan Radosavljevic, Fang-Chieh Chou, Tsung-Han Lin, Thi Nguyen, Tzu-Kuo Huang, Jeff Schneider, and Nemanja Djuric. Multimodal trajectory predictions for autonomous driving using deep convolutional networks. In *2019 International Conference on Robotics and Automation (ICRA)*, pages 2090–2096. IEEE, 2019.
- [8] Valentin De Bortoli, James Thornton, Jeremy Heng, and Arnaud Doucet. Diffusion schrödinger bridge with applications to score-based generative modeling. *Advances in Neural Information Processing Systems*, 34:17695–17709, 2021.
- [9] Prafulla Dhariwal and Alex Nichol. Diffusion models beat gans on image synthesis. In *Advances in Neural Information Processing Systems*, pages 8780–8794, 2021.
- [10] Nemanja Djuric, Vladan Radosavljevic, Henggang Cui, Thi Nguyen, Fang-Chieh Chou, Tsung-Han Lin, and Jeff Schneider. Short-term motion prediction of traffic actors for autonomous driving using deep convolutional networks. *arXiv preprint arXiv:1808.05819*, 1(2):6, 2018.

- [11] Ian Goodfellow, Jean Pouget-Abadie, Mehdi Mirza, Bing Xu, David Warde-Farley, Sherjil Ozair, Aaron Courville, and Yoshua Bengio. Generative adversarial nets. *Advances in neural information processing systems*, 27, 2014.
- [12] Chuan Guo, Shihao Zou, Xinxin Zuo, Sen Wang, Wei Ji, Xingyu Li, and Li Cheng. Generating diverse and natural 3d human motions from text. In *Proceedings of the IEEE/CVF Conference on Computer Vision and Pattern Recognition*, pages 5152–5161, 2022.
- [13] Agrim Gupta, Justin Johnson, Li Fei-Fei, Silvio Savarese, and Alexandre Alahi. Social gan: Socially acceptable trajectories with generative adversarial networks. In *Proceedings of the IEEE conference on computer vision and pattern recognition*, pages 2255–2264, 2018.
- [14] William Harvey, Saeid Naderiparizi, Vaden Masrani, Christian Weilbach, and Frank Wood. Flexible diffusion modeling of long videos. *Advances in Neural Information Processing Systems*, 35:27953–27965, 2022.
- [15] Jonathan Ho, Ajay Jain, and Pieter Abbeel. Denoising diffusion probabilistic models. In *Advances in Neural Information Processing Systems*, 2020.
- [16] Aapo Hyvärinen and Peter Dayan. Estimation of non-normalized statistical models by score matching. *Journal of Machine Learning Research*, 6(4), 2005.
- [17] Michael Janner, Yilun Du, Joshua B Tenenbaum, and Sergey Levine. Planning with diffusion for flexible behavior synthesis. *arXiv preprint arXiv:2205.09991*, 2022.
- [18] Tero Karras, Miika Aittala, Timo Aila, and Samuli Laine. Elucidating the design space of diffusion-based generative models. In Alice H. Oh, Alekh Agarwal, Danielle Belgrave, and Kyunghyun Cho, editors, *Advances in Neural Information Processing Systems*, 2022.
- [19] Dongjun Kim, Yeongmin Kim, Wanmo Kang, and Il-Chul Moon. Refining generative process with discriminator guidance in score-based diffusion models. *arXiv preprint arXiv:2211.17091*, 2022.
- [20] Diederik P Kingma and Jimmy Ba. Adam: A method for stochastic optimization. *arXiv preprint arXiv:1412.6980*, 2014.
- [21] Zhifeng Kong and Kamalika Chaudhuri. Data redaction from pre-trained gans. In *2023 IEEE Conference on Secure and Trustworthy Machine Learning (SaTML)*, pages 638–677. IEEE, 2023.
- [22] Namhoon Lee, Wongun Choi, Paul Vernaza, Christopher B Choy, Philip HS Torr, and Manmohan Chandraker. Desire: Distant future prediction in dynamic scenes with interacting agents. In *Proceedings of the IEEE conference on computer vision and pattern recognition*, pages 336–345, 2017.
- [23] Sergey Levine. Reinforcement learning and control as probabilistic inference: Tutorial and review. *arXiv preprint arXiv:1805.00909*, 2018.
- [24] Xingchao Liu, Lemeng Wu, Mao Ye, et al. Learning diffusion bridges on constrained domains. In *The Eleventh International Conference on Learning Representations*, 2023.
- [25] Pablo Alvarez Lopez, Michael Behrisch, Laura Bieker-Walz, Jakob Erdmann, Yun-Pang Flötteröd, Robert Hilbrich, Leonhard Lücken, Johannes Rummel, Peter Wagner, and Evamarie Wießner. Microscopic traffic simulation using sumo. In *2018 21st international conference on intelligent transportation systems (ITSC)*, pages 2575–2582. IEEE, 2018.
- [26] Saeid Naderiparizi, Adam Scibior, Andreas Munk, Mehrdad Ghadiri, Atilim Gunes Baydin, Bradley J Gram-Hansen, Christian A Schroeder De Witt, Robert Zinkov, Philip Torr, Tom Rainforth, et al. Amortized rejection sampling in universal probabilistic programming. In *International Conference on Artificial Intelligence and Statistics*, pages 8392–8412. PMLR, 2022.

- [27] Jiquan Ngiam, Benjamin Caine, Vijay Vasudevan, Zhengdong Zhang, Hao-Tien Lewis Chiang, Jeffrey Ling, Rebecca Roelofs, Alex Bewley, Chenxi Liu, Ashish Venugopal, et al. Scene transformer: A unified architecture for predicting multiple agent trajectories. *arXiv preprint arXiv:2106.08417*, 2021.
- [28] Alexander Quinn Nichol and Prafulla Dhariwal. Improved denoising diffusion probabilistic models. In *International Conference on Machine Learning*, pages 8162–8171. PMLR, 2021.
- [29] Niki Parmar, Ashish Vaswani, Jakob Uszkoreit, Lukasz Kaiser, Noam Shazeer, Alexander Ku, and Dustin Tran. Image transformer. In *International conference on machine learning*, pages 4055–4064. PMLR, 2018.
- [30] Alec Radford, Jong Wook Kim, Chris Hallacy, Aditya Ramesh, Gabriel Goh, Sandhini Agarwal, Girish Sastry, Amanda Askell, Pamela Mishkin, Jack Clark, et al. Learning transferable visual models from natural language supervision. In *International conference on machine learning*, pages 8748–8763. PMLR, 2021.
- [31] Hannes Risken and Hannes Risken. *Fokker-planck equation*. Springer, 1996.
- [32] Robin Rombach, Andreas Blattmann, Dominik Lorenz, Patrick Esser, and Björn Ommer. High-resolution image synthesis with latent diffusion models. In *Proceedings of the IEEE/CVF Conference on Computer Vision and Pattern Recognition*, pages 10684–10695, 2022.
- [33] Adam Ścibior, Vasileios Lioutas, Daniele Reda, Peyman Bateni, and Frank Wood. Imagining the road ahead: Multi-agent trajectory prediction via differentiable simulation. In *2021 IEEE International Intelligent Transportation Systems Conference (ITSC)*, pages 720–725. IEEE, 2021.
- [34] Peter Shaw, Jakob Uszkoreit, and Ashish Vaswani. Self-attention with relative position representations. *arXiv preprint arXiv:1803.02155*, 2018.
- [35] Jascha Sohl-Dickstein, Eric Weiss, Niru Maheswaranathan, and Surya Ganguli. Deep unsupervised learning using nonequilibrium thermodynamics. In *International Conference on Machine Learning*, pages 2256–2265. PMLR, 2015.
- [36] Jiaming Song, Chenlin Meng, and Stefano Ermon. Denoising diffusion implicit models. In *International Conference on Learning Representations*, 2020.
- [37] Yang Song and Stefano Ermon. Generative modeling by estimating gradients of the data distribution. In *Proceedings of the 33rd International Conference on Neural Information Processing Systems*, pages 11918–11930, 2019.
- [38] Yang Song, Jascha Sohl-Dickstein, Diederik P Kingma, Abhishek Kumar, Stefano Ermon, and Ben Poole. Score-based generative modeling through stochastic differential equations. In *International Conference on Learning Representations*, 2021.
- [39] Shuhan Tan, Kelvin Wong, Shenlong Wang, Sivabalan Manivasagam, Mengye Ren, and Raquel Urtasun. Scenegen: Learning to generate realistic traffic scenes. In *Proceedings of the IEEE/CVF Conference on Computer Vision and Pattern Recognition*, pages 892–901, 2021.
- [40] Guy Tevet, Sigal Raab, Brian Gordon, Yoni Shafir, Daniel Cohen-or, and Amit Haim Bermano. Human motion diffusion model. In *The Eleventh International Conference on Learning Representations*, 2023.
- [41] Ashish Vaswani, Noam Shazeer, Niki Parmar, Jakob Uszkoreit, Llion Jones, Aidan N Gomez, Łukasz Kaiser, and Illia Polosukhin. Attention is all you need. *Advances in neural information processing systems*, 30, 2017.
- [42] Pascal Vincent. A connection between score matching and denoising autoencoders. *Neural computation*, 23(7):1661–1674, 2011.
- [43] Andrew Warrington, Saeid Naderiparizi, and Frank Wood. Coping with simulators that don’t always return. In *International Conference on Artificial Intelligence and Statistics*, pages 1748–1758. PMLR, 2020.

- [44] Christian Weilbach, William Harvey, and Frank Wood. Graphically structured diffusion models. *arXiv preprint arXiv:2210.11633*, 2022.
- [45] Kan Wu, Houwen Peng, Minghao Chen, Jianlong Fu, and Hongyang Chao. Rethinking and improving relative position encoding for vision transformer. In *Proceedings of the IEEE/CVF International Conference on Computer Vision*, pages 10033–10041, 2021.
- [46] QI Yang and Haris N Koutsopoulos. A microscopic traffic simulator for evaluation of dynamic traffic management systems. *Transportation Research Part C: Emerging Technologies*, 4(3): 113–129, 1996.
- [47] Ye Yuan, Jiaming Song, Umar Iqbal, Arash Vahdat, and Jan Kautz. Physdiff: Physics-guided human motion diffusion model. *arXiv preprint arXiv:2212.02500*, 2022.
- [48] Chiyuan Zhang, Samy Bengio, Moritz Hardt, Benjamin Recht, and Oriol Vinyals. Understanding deep learning (still) requires rethinking generalization. *Communications of the ACM*, 64(3): 107–115, 2021.
- [49] Berend Zwartsenberg, Adam Scibior, Matthew Niedoba, Vasileios Lioutas, Justice Sefas, Yunpeng Liu, Setareh Dabiri, Jonathan Wilder Lavington, Trevor Campbell, and Frank Wood. Conditional permutation invariant flows. *Transactions on Machine Learning Research*, 2023. ISSN 2835-8856. URL <https://openreview.net/forum?id=DUsGpi3oCC>.

A Proofs

A.1 Proof of Theorem 1

Proof. Let α and $(1 - \alpha)$ be the prior probabilities of positive and negative examples under $p_\theta(\mathbf{x}_t; t)$. Note that α remains independent of t because

$$\begin{aligned}\alpha &= \int p_\theta(\mathbf{x}_t; t) p_\theta(\mathbf{x}_0 | \mathbf{x}_t) p_\theta(y = 1 | \mathbf{x}_0) d\mathbf{x}_0 d\mathbf{x}_t = \int p_\theta(\mathbf{x}_t; t) p_\theta(\mathbf{x}_0 | \mathbf{x}_t) \mathcal{O}(\mathbf{x}_0) d\mathbf{x}_0 d\mathbf{x}_t \\ &= \int p_\theta(\mathbf{x}_0, \mathbf{x}_t; t) \mathcal{O}(\mathbf{x}_0) d\mathbf{x}_0 d\mathbf{x}_t = \int p_\theta(\mathbf{x}_0; 0) \mathcal{O}(\mathbf{x}_0) d\mathbf{x}_0.\end{aligned}$$

The objective in Eq. (10) is equal to

$$\begin{aligned}-\mathbb{E}_t \left[\mathbb{E}_{p_\theta(\mathbf{x}_t)} \left[\mathbb{E}_{p_\theta(\mathbf{x}_0 | \mathbf{x}_t)} [\mathcal{O}(\mathbf{x}_0)] \log C_\phi(\mathbf{x}_t; t) + \mathbb{E}_{p_\theta(\mathbf{x}_0 | \mathbf{x}_t)} [(1 - \mathcal{O}(\mathbf{x}_0))] \log(1 - C_\phi(\mathbf{x}_t; t))] \right] \\ = -\mathbb{E}_t \left[\mathbb{E}_{p_\theta(\mathbf{x}_t)} [p(y = 1 | \mathbf{x}_t) \log C_\phi(\mathbf{x}_t; t) + p(y = 0 | \mathbf{x}_t) \log(1 - C_\phi(\mathbf{x}_t; t))] \right] \quad (15)\end{aligned}$$

This is equivalent to Eq. (7) after replacing q with p_θ , i.e. sampling from the reverse process instead of the forward. Therefore, its optimal solution follows Eq. (8). Hence,

$$\begin{aligned}\nabla_{\mathbf{x}_t} \log p_\theta(\mathbf{x}_t; t) + \nabla_{\mathbf{x}_t} \log C_{\phi^*}(\mathbf{x}_t; t) \\ = \nabla_{\mathbf{x}_t} \log p_\theta(\mathbf{x}_t; t) + \nabla_{\mathbf{x}_t} \log \alpha p_\theta(\mathbf{x} | y = 1; t) \\ \quad - \nabla_{\mathbf{x}_t} \log \left[\overbrace{\alpha p_\theta(\mathbf{x}_t | y = 1; t) + (1 - \alpha) p_\theta(\mathbf{x}_t | y = 0; t)}^{p_\theta(\mathbf{x}_t; t)} \right] \\ = \nabla_{\mathbf{x}_t} \log \alpha p_\theta(\mathbf{x}_t | y = 1; t) = \nabla_{\mathbf{x}_t} \log p_\theta(\mathbf{x}_t | y = 1; t)\end{aligned}$$

□

A.2 Proof of Corollary 1.1

Proof. Since p_{θ, ϕ^*} is defined as the distribution generated by simulating the SDE in equation 2, its score function $\nabla_{\mathbf{x}_t} \log p_{\theta, \phi^*}(\mathbf{x}_t; t)$ is by definition equal to $s_{\theta, \phi^*}(\mathbf{x}_t; t)$ [31, 37]. Similarly for the baseline DM we have $s_\theta(\mathbf{x}_t; t) = \nabla_{\mathbf{x}_t} p_\theta(\mathbf{x}_t; t)$. Therefore,

$$\nabla_{\mathbf{x}_t} \log p_{\theta, \phi^*}(\mathbf{x}_t; t) = s_{\theta, \phi^*}(\mathbf{x}_t; t) \stackrel{\text{Eq. (9)}}{=} s_\theta(\mathbf{x}_t; t) + \nabla_{\mathbf{x}_t} \log C_{\phi^*}(\mathbf{x}_t; t) \quad (16)$$

$$= \nabla_{\mathbf{x}_t} \log p_\theta(\mathbf{x}_t; t) + \nabla_{\mathbf{x}_t} \log C_{\phi^*}(\mathbf{x}_t; t) \stackrel{\text{Thm. 1}}{=} \nabla_{\mathbf{x}_t} \log p_\theta(\mathbf{x}_t | y = 1) \quad (17)$$

Here we derived $s_{\theta, \phi^*}(\mathbf{x}_t; t) = \nabla_{\mathbf{x}_t} \log p_\theta(\mathbf{x}_t | y = 1)$. By [1], we proved the first statement.

The second statement follows by decomposing $p_\theta(\mathbf{x}_t | y = 1)$:

$$p_{\theta, \phi^*}(\mathbf{x}) = p_\theta(\mathbf{x} | y = 1) \propto p_\theta(\mathbf{x}) \mathcal{O}(\mathbf{x}) \quad \Rightarrow \quad p_{\theta, \phi^*}(\mathbf{x}) = 0 \quad \forall \mathbf{x} \in \Omega^c.$$

For the last statement, we have

$$\left. \begin{aligned}p_{\theta, \phi^*}(\mathbf{x}) &= \frac{p_\theta(\mathbf{x}) \mathcal{O}(\mathbf{x})}{\int p_\theta(\mathbf{x}) \mathcal{O}(\mathbf{x}) d\mathbf{x}} \\ \int p_\theta(\mathbf{x}) \mathcal{O}(\mathbf{x}) d\mathbf{x} &\leq 1\end{aligned} \right\} \Rightarrow p_{\theta, \phi^*}(\mathbf{x}) \geq p_\theta(\mathbf{x}) \quad \forall \mathbf{x} \in \Omega$$

$$\stackrel{\mathcal{D} \subseteq \Omega}{\Rightarrow} \log p_{\theta, \phi^*}(\mathcal{D}) = \sum_{\mathbf{x} \in \mathcal{D}} \log p_{\theta, \phi^*}(\mathbf{x}) \geq \sum_{\mathbf{x} \in \mathcal{D}} \log p_\theta(\mathbf{x}) = \log p_\theta(\mathcal{D}).$$

□

We demonstrate this corollary with a one-dimension density in Fig. 4. We show a ‘‘base distribution’’ $p(x)$ and the positive and negative regions Ω and Ω^c , respectively. We can see that the distribution $p(x | y = 1)$ assigns no mass to Ω^c and has a larger mass assigned to any point in Ω .

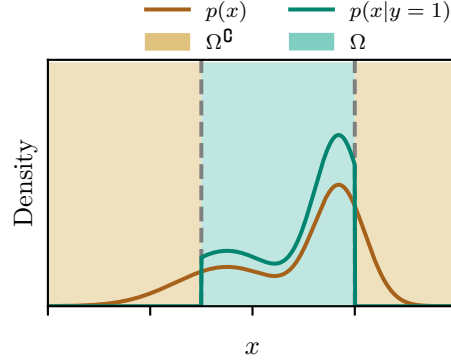


Figure 4: We use this one-dimensional density plot to show how we guide the generation process towards the positive support region indicated by the oracle. The original density curve $p(x)$ is a mixture of two Gaussian distributions, and we depicts the region in cyan as the eligible support restricted by oracle function, otherwise in buff. Ideally, the well-behaved Bayes optimal classifier helps to target exactly the score function of oracle-approved examples such that the resulting density function $p(x|y = 1)$ only lands in the cyan area and assigns zero probability outside this region.

A.3 Equivalence of cross-entropy loss minimization and KL divergence minimization

Claim: minimizing the cross-entropy loss between the classifier output and the true label is equivalent to minimizing the KL divergence between the classifier output and the Bayes optimal classifier.

Proof. The Bayes optimal classifier $C^*(\mathbf{x}_t; t)$ approximates $q(y = 1|\mathbf{x}_t)$. Let $p_\phi(y|\mathbf{x}_t)$ be the distribution represented by the learned classifier $C_\phi(\mathbf{x}_t; t)$ i.e., $p_\phi(y = 1|\mathbf{x}_t) = C_\phi(\mathbf{x}_t; t)$. For an arbitrary diffusion time step t , the expected KL divergence between the Bayes optimal and the learned classifier therefore is

$$\begin{aligned} & \mathbb{E}_{q(\mathbf{x}_t)} [\text{KL}(q(y|\mathbf{x}_t)||p_\phi(y|\mathbf{x}_t))] \\ &= \mathbb{E}_{q(\mathbf{x}_t)} \left[\mathbb{E}_{q(y|\mathbf{x}_t)} \left[q(y|\mathbf{x}_t) \log \frac{q(y|\mathbf{x}_t)}{p_\phi(y|\mathbf{x}_t)} \right] \right] \end{aligned} \quad (18)$$

$$= \mathbb{E}_{q(\mathbf{x}_t)} \left[q(y = 1|\mathbf{x}_t) \log \frac{q(y = 1|\mathbf{x}_t)}{C_\phi(\mathbf{x}_t; t)} + q(y = 0|\mathbf{x}_t) \log \frac{q(y = 0|\mathbf{x}_t)}{1 - C_\phi(\mathbf{x}_t; t)} \right] \quad (19)$$

$$= \mathbb{E}_{q(\mathbf{x}_t)} [H(q(y|\mathbf{x}_t))] - \mathbb{E}_{q(\mathbf{x}_t)} [q(y = 1|\mathbf{x}_t) \log C_\phi(\mathbf{x}_t; t) + q(y = 0|\mathbf{x}_t) \log(1 - C_\phi(\mathbf{x}_t; t))]. \quad (20)$$

The first term is the expected entropy of the optimal classifier and is independent of ϕ . Therefore,

$$\begin{aligned} & \arg \min_{\phi} \mathbb{E}_{q(\mathbf{x}_t)} [\text{KL}(q(y|\mathbf{x}_t)||p_\phi(y|\mathbf{x}_t))] \\ &= \arg \min_{\phi} -\mathbb{E}_{q(\mathbf{x}_t)} [q(y = 1|\mathbf{x}_t) \log C_\phi(\mathbf{x}_t; t) + q(y = 0|\mathbf{x}_t) \log(1 - C_\phi(\mathbf{x}_t; t))] \end{aligned} \quad (21)$$

$$= \arg \min_{\phi} \text{CE}(q(y|\mathbf{x}_t), p_\phi(y|\mathbf{x}_t)). \quad (22)$$

□

Note that Eq. (7) is the expected cross entropy for different time steps t .

A.4 Connection between Eq. (10) and Eq. (12)

In this section we make the connection between Eq. (7) and Gen-neG's objective (Eq. (12)) more clear. The objective in Eq. (10), ignoring the outer expectation with respect to t , is equal to

$$- \left(\mathbb{E}_{p_\theta(\mathbf{x}_0, \mathbf{x}_t)} [\mathcal{O}(\mathbf{x}_0) \log C_\phi(\mathbf{x}_t; t) + (1 - \mathcal{O}(\mathbf{x}_0)) \log(1 - C_\phi(\mathbf{x}_t; t))] \right) \quad (23)$$

$$= - \int p_\theta(\mathbf{x}_0, \mathbf{x}_t) \left(p(y=1|\mathbf{x}_0) \log C_\phi(\mathbf{x}_t; t) + p(y=0|\mathbf{x}_0) \log(1 - C_\phi(\mathbf{x}_t; t)) \right) d\mathbf{x}_0 d\mathbf{x}_t \quad (24)$$

$$= - \int p_\theta(y=1) p_\theta(x_0|y=1) p_\theta(x_t|x_0) \log C_\phi(\mathbf{x}; t) d\mathbf{x}_0 d\mathbf{x}_t \\ + \int p_\theta(y=0) p_\theta(x_0|y=0) p_\theta(x_t|x_0) \log(1 - C_\phi(\mathbf{x}_t; t)) d\mathbf{x}_0 d\mathbf{x}_t \quad (25)$$

$$\approx - \int p_\theta(y=1) p_\theta(x_0|y=1) q(x_t|x_0) \log C_\phi(\mathbf{x}; t) d\mathbf{x}_0 d\mathbf{x}_t \\ + \int p_\theta(y=0) p_\theta(x_0|y=0) q(x_t|x_0) \log(1 - C_\phi(\mathbf{x}_t; t)) d\mathbf{x}_0 d\mathbf{x}_t \quad (26)$$

$$= p(y=1) \mathbb{E}_{p_\theta(\mathbf{x}_0|y=1)} \left[\mathbb{E}_{q(\mathbf{x}_t|\mathbf{x}_0)} [-\log C_\phi(\mathbf{x}_t; t)] \right] \\ + p(y=0) \mathbb{E}_{p_\theta(\mathbf{x}_0|y=0)} \left[\mathbb{E}_{q(\mathbf{x}_t|\mathbf{x}_0)} [-\log(1 - C_\phi(\mathbf{x}_t; t))] \right] \quad (27)$$

Noting that $\alpha := p(y=1)$ recovers Eq. (12).

A.5 Gen-neG’s objective function

Here we show why Eq. (13) is an importance sampling estimator of the original objective function in Eq. (12).

$$\mathcal{L}_\phi^{\text{cls}}(\alpha) := \alpha \mathbb{E}_{p_\theta(\mathbf{x}_0|y=1)} \left[\mathbb{E}_{q(\mathbf{x}_t|\mathbf{x}_0)} [-\log C_\phi(\mathbf{x}_t; t)] \right] \\ + (1 - \alpha) \mathbb{E}_{p_\theta(\mathbf{x}_0|y=0)} \left[\mathbb{E}_{q(\mathbf{x}_t|\mathbf{x}_0)} [-\log(1 - C_\phi(\mathbf{x}_t; t))] \right] \quad (28)$$

$$= - \mathbb{E}_{p_\theta(y)} \left[\mathbb{E}_{p_\theta(\mathbf{x}_0|y)} \left[\mathbb{E}_{q(\mathbf{x}_t|\mathbf{x}_0)} [y \log C_\phi(\mathbf{x}_t; t) + (1 - y) \log(1 - C_\phi(\mathbf{x}_t; t))] \right] \right]. \quad (29)$$

Now we apply importance sampling to $p_\theta(y)$ by sampling from $\pi(y)$ as the proposal distribution. Therefore,

$$\mathcal{L}_\phi^{\text{cls}}(\alpha) = - \mathbb{E}_{p_\theta(y)} \left[\mathbb{E}_{p_\theta(\mathbf{x}_0|y)} \left[\mathbb{E}_{q(\mathbf{x}_t|\mathbf{x}_0)} [y \log C_\phi(\mathbf{x}_t; t) + (1 - y) \log(1 - C_\phi(\mathbf{x}_t; t))] \right] \right] \quad (30)$$

$$= - \mathbb{E}_{\pi(y)} \left[\frac{p_\theta(y)}{\pi(y)} \mathbb{E}_{p_\theta(\mathbf{x}_0|y)} \left[\mathbb{E}_{q(\mathbf{x}_t|\mathbf{x}_0)} [y \log C_\phi(\mathbf{x}_t; t) + (1 - y) \log(1 - C_\phi(\mathbf{x}_t; t))] \right] \right] \quad (31)$$

$$= \frac{p_\theta(y=1)}{\pi(y=1)} \mathbb{E}_{p_\theta(\mathbf{x}_0|y=1)} \left[\mathbb{E}_{q(\mathbf{x}_t|\mathbf{x}_0)} [-\log C_\phi(\mathbf{x}_t; t)] \right] \\ + \frac{p_\theta(y=0)}{\pi(y=0)} \mathbb{E}_{p_\theta(\mathbf{x}_0|y=0)} \left[\mathbb{E}_{q(\mathbf{x}_t|\mathbf{x}_0)} [-\log(1 - C_\phi(\mathbf{x}_t; t))] \right] \quad (32)$$

$$= \mathbb{E}_{p_\theta(\mathbf{x}_0|y=1)} \left[\frac{\alpha}{\pi(y=1)} \mathbb{E}_{q(\mathbf{x}_t|\mathbf{x}_0)} [-\log C_\phi(\mathbf{x}_t; t)] \right] \\ + \mathbb{E}_{p_\theta(\mathbf{x}_0|y=0)} \left[\frac{1 - \alpha}{\pi(y=0)} \mathbb{E}_{q(\mathbf{x}_t|\mathbf{x}_0)} [-\log(1 - C_\phi(\mathbf{x}_t; t))] \right] \quad (33)$$

In our case, $\pi(y)$ is a uniform Bernoulli distribution i.e., $\pi(y=1) = \pi(y=0) = 0.5$. Therefore, minimizing Eq. (13) is equivalent to minimizing a Mone Carlo estimate of Eq. (33).

B Experimental details

B.1 Toy Experiment

Architecture We use a fully connected network with 2 residual blocks as shown in Fig. 5. The hidden layer size in our experiment is 256 and timestep embeddings (output of the sinusoidal embedding layer) is 128. Our classifier has a similar architecture, the only difference is that the classifier has a different output dimension of one. Our baseline DM and classifier networks both have around 330k parameters.



Figure 5: Architecture of the network in the toy experiment. Left: the overall of the model. Right: detailed architecture of our “Residual Block”. In this architecture, timestep is embedded using sinusoidal embedding and all nonlinearities are SiLU. The output of the network $F_\theta(\mathbf{x}_t, t)$ is then used in a preconditioning function to get an estimate of \mathbf{x}_0 .

Training the baseline DM We train our models baseline models on a single GPU, (we use either of GeForce GTX 1080 Ti or GeForce GTX TITAN X) for 30,000 iterations. We use the Adam optimizer [20] with a batch size of 3×10^{-4} and full-batch training i.e., our batch size is 1000 which is the same as the training dataset size.

Training the classifiers Each classifier is trained on a fully-synthetic dataset of 100k samples which consists of 50k positive and 50k negative samples. This dataset is generated with 100 diffusion steps. We train the classifier for 20k iterations with a batch size of 8192. We use Adam optimizer with a learning rate of 3×10^{-3} .

Distillation The distilled models have the same architecture and hyperparameters as the baseline DM model. They are trained for 250k iterations on the true dataset with a batch size of 1000. We use Adam optimizer with a learning rate of 3×10^{-4} .

Diffusion process We use the EDM framework in this experiment with a preconditioning similar to the one proposed in Karras et al. [18]. In particular, the following preconditioning is applied to the network in Fig. 5, called $F_\theta(\mathbf{x}_t, t)$, to get $D_\theta(\mathbf{x}_t; t)$ which returns an estimate of \mathbf{x}_0 .

$$D_\theta(\mathbf{x}_t; t) = \frac{\sigma_{\text{data}}^2}{\sigma(t)^2 + \sigma_{\text{data}}^2} \mathbf{x}_t + \sigma(t) F_\theta \left(\frac{1}{\sqrt{\sigma(t)^2 + \sigma_{\text{data}}^2}} \mathbf{x}_t; \frac{1}{4} \ln(\sigma(t)) \right). \quad (34)$$

Following [18], we simply let $\sigma_{\text{data}} = 0.5$.

In total, we spent around 250 GPU-hours for this experiment.

B.2 Infractions in Traffic Scene Generation

Overview This section provides additional details for the traffic scene generation task. The architecture for training the baseline DM model, classifiers and distillation models is majorly based on transformers introduced by Vaswani et al. [41]. In particular, the architecture backbone consists of an encoder, a stack of attention residual blocks, and a decoder. Each of them will be discussed in detail later. The original data input shape is $[B, A, F]$ corresponding to A vehicles and F feature dimensions in a batch with B many scenes.

In terms of parameters, the attention layers comprise the majority portion of the entire architectures so that the difference in decoder is relatively small, and the resulting architectures all contain approximately 6.3 million parameters. We use NVIDIA A100 GPUs for training and validating models, synthetic datasets generation with around 400 GPU-hours in total. We train each model with a batch size of 64 and Adam optimizer with a learning rate of 10^{-4} .

Encoder and time embeddings To generate input features, we use sinusoidal positional embeddings to embed the diffusion time and 2-layer MLP with activation function SiLU to embed the original data separately into $H = 196$ hidden feature dimensions. The sum of the two embeddings is the input that is fed into the attention-based architecture.

Self-attention Layer and Cross-attention Layer The major implementation of multi-head ($k = 4$) attention blocks is built on Transformer [41]. Applying self-attention across agents enables model to learn the multi-agent interactions, while applying map-conditional cross-attention between agents and map allows agents to interact with the road representations. To prepare road image for model input, we use a convolutional neural network and a feed-forward network [5] to generate a lower-resolution map $m' \in \mathbb{R}^{196 \times 32 \times 32}$ from the original image $m \in \mathbb{R}^{3 \times 256 \times 256}$. Since the transformer architecture is permutation-invariant, we add a 2D positional encoding [29, 4] based on m' on the top of the map representation to preserve the spatial information of the image.

Relative Positional Encodings (RPEs) During experiments, we find the collision rate is much higher than the offroad rate. In order to effectively lower the frequency of or completely avoid vehicle collision occurrence, we attempt to capture the relative positions by performing relative positional encodings (RPEs) in self-attention residual blocks and enforce the vehicles being aware of the other vehicles in close proximity in each scene. Following [34, 45, 14], we compute the distances of each pair of vehicles and summarise into a tensor of shape $[B, A, A]$, where d_{ij}^b is the distance between vehicle i and j in the b^{th} scene. We choose to use sinusoidal embeddings (similar to how we embed diffusion time t) to parameterize d_{ij}^b rather than logarithm function $f_{\text{RPE}}(d_{ij}^b) = \log(1 + d_{ij}^b)$, as we need to adequately amplify the pairwise distances between vehicles when it is comparably small. We perform this operation together with diffusion time embedding at each diffusion time step, and we regard their sum as the complete pairwise distance embeddings. The resulting embedding tensor \mathbf{p} is of the shape $[B, A, A, H]$, where \mathbf{p}_{ij}^b is the encoding vector of length H representing the pairwise distance of vehicle i and j in the b^{th} scene.

In each scene, we have an input sequence, $\mathbf{x} = (\mathbf{x}_1, \dots, \mathbf{x}_A)$, and each \mathbf{x}_i is linearly transformed to query $\mathbf{q}_i = W^Q \mathbf{x}_i$, key $\mathbf{k}_i = W^K \mathbf{x}_i$ and value $\mathbf{v}_i = W^V \mathbf{x}_i$. We also apply linear transformation onto RPEs to obtain query $\mathbf{p}_{ij}^Q = U^Q \mathbf{p}_{ij}$, key $\mathbf{p}_{ij}^K = U^K \mathbf{p}_{ij}$ and value $\mathbf{p}_{ij}^V = U^V \mathbf{p}_{ij}$. Then the add-on output from the self-attention residual block is the aggregated outputs of the vanilla transformer and the relative-position-aware transformer:

$$\mathbf{x}_i^{\text{output}} = \mathbf{x}_i + \sum_{j=1}^A \alpha_{ij} (\mathbf{v}_j + \mathbf{p}_{ij}^V) \quad (35)$$

$$\text{where } \alpha_{ij} = \frac{\exp(e_{ij})}{\sum_{k=1}^A \exp(e_{ik})} \text{ and } e_{ij} = \frac{\mathbf{q}_i^\top \mathbf{k}_j + \mathbf{p}_{ij}^Q \mathbf{k}_j + \mathbf{q}_i^\top \mathbf{p}_{ij}^K}{\sqrt{d_{\mathbf{x}}}} \quad (36)$$

Decoder The settings for baseline, distillation models and classifiers are almost identical except the decoder for producing the final output. For baseline and distillation models, we apply 2-layer MLP and reconstruct the output of the shape $[B, A, H]$ from the final attention layer into $[B, A, D]$ through the decoder. To ensure we output individual label for each vehicle with by-agent classifiers, and a collective label for a scene with by-scene classifiers, and we conduct the operations as follows. The decoder takes the hidden representation of the shape $[B, A, H]$ and produces a tensor with feature dimension $F' = 1$ with a 2-layer MLP, which is the predicted labels from the by-agent classifiers. For by-scene classifier, we add additional MLP layer to extract the first column from the second dimension of the by-agent classifier resulting predictions and obtain a tensor of the shape $[B, 1, 1]$.

B.3 Motion Diffusion

We used the official implementation of MDM² for our Motion Diffusion experiment. For the baseline DM, we used their officially released best pretrained checkpoint of text to motion task on HumanML3D dataset. We generate a synthetic dataset of around 250k positive and 250k negative examples from the baseline DM which is a DDPM-based model with 1000 diffusion steps. We then

²<https://github.com/GuyTevet/motion-diffusion-model>

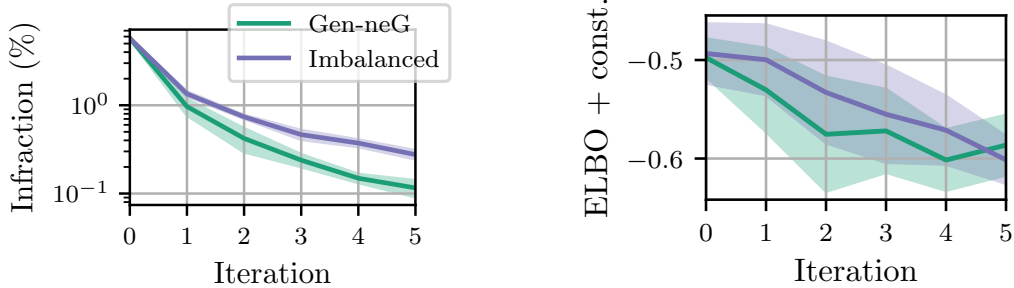


Figure 6: Infraction and ELBO estimations from different iterations of Gen-neG and an ablated version of it without label imbalance correction. Gen-neG achieves a lower infraction rate and a comparable ELBO.

define our classifier architecture using their code base. Following our other experiments, our classifier architecture is the same as the baseline DM model. We train the classifier with a batch size of 256 and a learning rate of 10^{-4} for 100k iterations. Otherwise, we use the same hyperparameters as in [40]. All the training and data generation is done on A100 GPUs.

To compute the FID scores, in accordance with [40], we generate one motion for each caption in the HumanML3D test set, resulting in a total of 4,626 generated motions. In contrast to [40], we refrain from applying classifier-free guidance during the sample generation process. Subsequently, we calculate the FID score between the generated motions and the ground-truth motions in the test set. The FID metric quantifies the distance in the latent space of a motion encoder, which has been pre-trained using contrastive learning [12].

The total compute used for this experiment (generating the datasets and training the classifiers) was around 600 GPU-hours.

C Additional results

C.1 Alternative approaches to conditional generation with diffusion models

In our journey towards solving this problem, we explored multiple different approaches. Here we briefly mention a few of the more promising ones.

Diffusion bridges Liu et al. [24] proposes a framework for diffusion modeling of constrained domains. Their proposed method requires adding a guidance term to the diffusion process which comes in form of an expectation. This expectation is only tractable for simple constraints such as the one in our toy experiment. We applied this method on our toy experiment which lead to practically zero infraction, without overfitting. As the update term is intractable for the larger scale experiment, we tried to learn an estimation of it, but we failed to reliably estimate the update term.

Learning in the joint space of (\mathbf{x}, y) Inspired by Weilbach et al. [44], we trained a model to estimate all the marginals and conditionals on the joint space of (\mathbf{x}, y) where $q(\mathbf{x}|y = 1)$ is the training set, $q(\mathbf{x}|y = 0)$ is a synthetically generated set of negative examples and $q(y = 1)$ is a hyper-parameter. We assign a probability vector for choosing a training task among learning conditional probabilities $q(\mathbf{x}|y)$, $q(y|x)$ and joint probability $q(\mathbf{x}, y)$ collectively with one architecture parameterized by θ with implicit classifier learner $p_\theta(y|x)$. Intuitively, feeding the model with both positive and negative samples helps the model learn the boundary between the positive region Ω and negative region Ω^c . At test time, we only sample from $p_\theta(\mathbf{x}|y = 1)$. Our preliminary results suggested that it helps reducing the infraction rate, but is outperformed by Gen-neG.

Table 3: Results for traffic scene generation, in terms of collision, offroad, and overall infractions as well as ELBO. Two varieties (“by-scene” and “by-agent”) for the classifier are presented, as well as results with (Gen-neG) and without importance sampling. The final two rows provide the results of distilling the models labelled with † and *.

Method	Collision (%) ↓	Offroad (%) ↓	Infraction (%) ↓	r-ELBO ($\times 10^2$) ↑
baseline DM	28.3 ± 0.70	1.3 ± 0.14	29.3 ± 0.64	-27.5 ± 0.01
by-scene	23.3 ± 0.7	1.0 ± 0.28	24.1 ± 0.67	-27.6 ± 0.01
by-scene imbalanced	23.8 ± 0.6	1.0 ± 0.3	24.6 ± 0.54	-27.6 ± 0.01
by-agent	16.4 ± 0.5	0.9 ± 0.12	17.2 ± 0.44	-27.7 ± 0.01
by-agent imbalanced	17.8 ± 1.21	0.9 ± 0.16	18.6 ± 1.3	-27.7 ± 0.01



Figure 7: Complete visualization comparisons for infraction in traffic scene generation experiments. Subplots show infraction per unit area under different models. The left-most is before Gen-neG is applied. The second is the a classifier added onto the baseline model. The third is a stack of classifiers added onto the baseline model. The last two are the distillation models trained to learn the baseline model with one classifier or a stack of classifiers. A clear reduction in terms of infractions per unit area can be observed from left to right.

C.2 Ablation on label imbalance

As mentioned in Section 3.2, naively generating synthetic datasets for training the classifier causes a major label imbalance issue hinders training of the classifier. In this section we perform an ablation study to empirically demonstrate its effect in our experiments.

As a reminder, Gen-neG guarantees an equal number of positive and negative examples in the synthetic datasets, and it employs importance sampling to address any distribution shift introduced. In the ablated experiment (referred to as “imbalanced” in the results), the ratio of positive to negative examples is model-dependent, being equal to the model’s infraction rate. It results in a gradual increase in the dominance of positive examples as the model’s infraction rate decreases.

Toy experiment We repeat our toy experiment with and without Gen-neG’s imbalance correction. In each iteration, we create a synthetic dataset of 20,000 samples and train a binary classifier for 10,000 iterations. The other details are the same as the experiment in the main text. We show the performance of these models in Fig. 6. We observe that “imbalanced”, the ablated version of Gen-neG, is consistently outperformed by Gen-neG in infraction rate. Furthermore, the performance gap between the two methods widens as the models improve. However, it is worth noting that Gen-neG achieves a comparable ELBO to that of “imbalanced” despite these infraction rate differences.

Traffic Scene Generation We conduct a similar ablation as described above, where we train classifiers on a imbalanced datasets of the same size as our method. The results of this ablated experiment are presented in Table 3, and they are compared with the results reported in the main text.

C.3 More visualization results for traffic scene generation

In Fig. 7 we report more visualization results from our traffic scene generation experiment. This figure follows from and adds more details to Fig. 1.

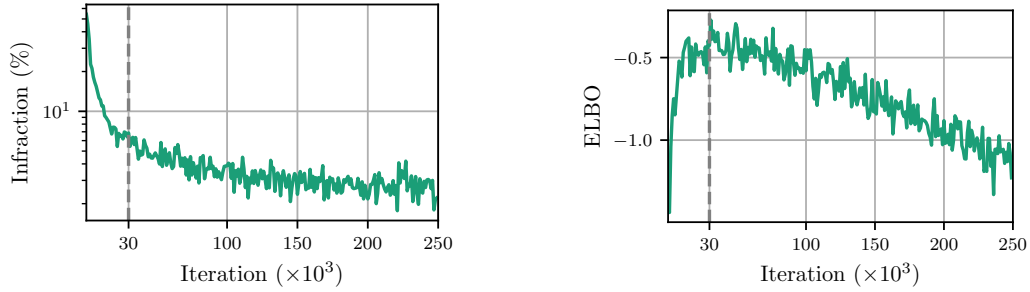


Figure 8: Overfitting results in the toy experiment. The plot on the left shows the infraction rate and the one on the right shows the ELBO on a held-out validation set. We observe that training baseline DM for longer can achieve much lower infraction rates that reported. However, it quickly starts to overfit, leading to poor ELBO estimates on the held-out validation set.

C.4 Overfitting in the toy experiment

Here we report our results for overfitting the baseline DM in the toy experiment. We run an experiment with 250,000 training iterations, much larger than the 30,000 iterations in the reported results. As we can see in Fig. 8, the infraction rate keeps decreasing. However, the model starts overfitting after around 30,000 iterations, as measure by the ELBO on a held-put set. This suggests that the architecture is expressive enough to model sharp jumps in the learned density. However, simply training it on a small dataset without incorporating any prior on “where to allocate its capacity” fails because the model does not receive any signal on where the actual “sharp jump” is. Gen-neG, on the other hand, provides this kind of signal through the oracle-assisted guidance.